A novel electrochemical immunosensor for ultrasensitive detection of tumor necrosis factor α based on polystyrene -PAMAM dendritic polymer blend nanofibers

Pouyan Razmshoar, S.H. Bahrami, Mohammad Rabiee, Marie Hangouet, Marie Martin, Abdelhamid Errachid, Nicole Jaffrezic-Renault

A novel electrochemical immunosensor for ultrasensitive detection of tumor necrosis factor α based on polystyrene - PAMAM dendritic polymer blend nanofibers

Pouyan Razmshoar[1], S. Hajir Bahrami[1*], Mohammad Rabiee[2], Marie Hangouet[3], Marie Martin[3], Abdelhamid Errachid[3], Nicole Jaffrezic-Renault[3*]

1. Textile Engineering Department, Amirkabir University of Technology (Tehran Polytechnic), Tehran, Iran

2. Biomedical Engineering Department, Amirkabir University of Technology (Tehran Polytechnic), Tehran, Iran

3. University of Lyon, Institute of Analytical Sciences, UMR 5280, CNRS, F-69100, Villeurbanne, France

Corresponding authors : S. Hajir Bahrami, hajirb@aut.ac.ir ; Nicole Jaffrezic-Renault, nicole.jaffrezic@univ-lyon1.fr

Abstract:

A simple, rapid, and highly sensitive label-free immunosensor based on polystyrene (PS)-polyamidoamine (PAMAM) dendritic polymer nanofibers (NFs) for detection of tumor necrosis factor-α (TNF-α) cytokine was developed. The choice of PAMAM was due to the possibility of designing the surface of NFs to create a novel interface with the high control ability of the density of amine groups at the surface by which capture antibody (anti-TNF-α) could be covalently attached to the surface of NFs through glutaraldehyde (GA) coupling chemistry. Evaluation of the electrode surface using cyclic voltammetry (CV) proved the electrode manufacturing stages were successful by decreasing the peak current values due to the blockage of electron transfer by the biomolecule layer on the surface of NFs, as well as the ability to precisely control the current peak by changing the diameter of the NFs and the concentration of dendrimer. Electrochemical impedance spectroscopy (EIS) was used to test the detection capability of the immunosensors and compare the role of the amount of PAMAM presented on the surface of NFs on their analytical performance. Increasing the concentration of dendrimer greatly increased the sensitivity of immunosensors due to the higher

stabilization of the antibody on the nanofiber surface. The immunosensor had a very high affinity for TNF-α cytokines, with a linear response ranging from 10 to 200 pg/mL and a low limit of detection (LOD) of 669 fg/mL. Interference results with Interleukin-10 (IL-10) cytokine showed that the immunosensor was extremely specific and may be utilized to detect cytokines in clinical diagnosis.

Keywords: Electrospun nanofibers, Polystyrene (PS), Polyamidoamine (PAMAM), Electrochemical impedance spectroscopy (EIS), immunosensor, tumor necrosis factor-α (TNF-α)

1. Introduction

Tumor Necrosis Factor-alpha (TNF-α) is a pro-inflammatory cytokine produced by lymphocytes and macrophages that has been implicated in the stimulation of the acute phase response, anticancer activity, and immune system regulation [1,2]. According to recent researches, TNF-α levels in a patient's blood plasma and saliva are linked to heart failure (HF), and it can be used as a specific biomarker in detecting the first signs of future cardiovascular events [3,4]. Since the concentration of TNF-α in healthy human serum is less than 10 pg/mL, and in the serum of patients with severe autoimmune diseases is between 10-300 pg/mL depending on the severity of the disease, accurate estimating its concentration in human fluids is a significant challenge and important to early diagnosis of disease [4,5]. Traditional methods such as ELISA for TNF-α detection have always disadvantages including long assay times, large sample volumes for analysis, the inability to assess in real time, and the necessity for a specialist. [6,7]. Electrochemical immunosensors have received much interest in recent years as an alternative to conventional approaches in TNF-α detection because of their high sensitivity, easy instrumentation, accuracy, and quick response [8–10].

In this work, based on two novel perspectives a highly sensitive electrochemical immunosensor for TNF-α cytokine detection was developed. First, the usage of the NFs structure in immunosensor construction with the goal of providing a diagnostic platform with a large surface area to immobilize TNF-α antibodies in

such a way that they have maximal TNF-α cytokine accessibility to improve immunosensor sensitivity. The use of NFs in the production of electrochemical immunosensors might lead to the development of a new generation of miniaturized immunosensors that can answer key issues of previous works such as increased sensitivity, simplicity, and rapid detection. Second, fiber surface engineering in terms of the kind and quantity of functional groups suited for covalent immobilization of TNF-α antibody with a specific distance to build a protein-friendly interface with high stability so that the analyte may be detected in the smallest amount feasible. PAMAM dendrimers are globular, highly branched polymeric macromolecules with a polyvalent core (ethylene diamine (EDA)), internal repeating branched units (amidoamine), and high terminal active surface groups [11,12]. Dendrimers provide the possibility of immobilizing bioreceptors for the design of immunosensors due to their unique structural and chemical features, such as multiple functional groups, hydrophilicity, high mechanical and chemical stability, and similar size to biomolecules [13,14]. Accordingly, great emphasis has been placed on the use of PAMAM in the production of extremely sensitive electrochemical immunosensors in order to speed up the electron transfer process, enhance antibody immobilization efficiency, and improve electrochemical responses and signal amplification [15–17]. A previous study on the modification of the ELISA kit surface using PAMAM for TNF-α cytokine detection showed increased sensitivity and the detection limit through better orientation of the antibodies compared to the commercially ELISA kit [18]. In this work, PS-PAMAM dendritic polymer NFs were produced for the first time, with doped PS and PAMAM dendritic polymer with different concentrations, then allowing covalent interaction with the Fc region of the TNF antibody after amine group activation. As a result, the impact of increasing PAMAM concentration on its presence on the fiber surface and TNF-α detection was investigated. Electrochemical impedance was utilized in the final step to detect changes in electron transport properties after the development of antibody–antigen immune complexes on the surface of NFs mats deposited on a gold electrode. The immunosensors' repeatability, reproducibility, and selectivity were all examined.

2. Materials and methods

2.1. Chemicals and Reagents

In the supplementary information, the reagents, instruments, and characterizations parts were described in detail.

2.2. PS and PS-PAMAM nanofibrous mats preparation

PS granules were dissolved in N,N,-dimethylformamide (DMF) solvent at room temperature (RT) under magnetic stirring overnight to prepare a 20 wt. % PS solution for electrospinning. The preparation of PS-PAMAM NFs mats with different mass ratios of 85-15, 75-25, and 65-35 was conducted in two step process. The precise quantities of PS and PAMAM dendritic polymer were dissolved separately in DMF solvent for each mass ratio. The overnight stirring was conducted at RT to obtain clear solutions. The PAMAM dendritic polymer solution was gently added to the PS solution in the second step, and the mixture was stirred for 4 h to obtain a PS-PAMAM 20 wt. % solution. After this step, PS-PAMAM solutions with different mass ratios were used immediately for electrospinning. The solutions were loaded into a 1ml syringe supplied with a laser-cut needle (22 gages) and fed through a polytetrafluoroethylene (PTFE) tube from the syringe to the nozzle using the syringe pump (electrospinning instrument, Spraybase®, Ireland). In order to obtain NFs with a bead-less morphology with uniformity in diameter, various parameters such as voltage, injection rate and distance from the nozzle to the collector were changed. The electrospinning parameters were 27 kV for the applied voltage, rate 0.25 ml/h and the tip-to-collector distance 20 cm.

After obtaining uniform and bead-less NFs, they were electrospun on the surface of gold electrode that was placed on a collector for 1min. Before electrospinning, the gold electrodes were placed in acetone for 15min and then in ethanol in an ultrasonic bath for 15min for cleaning. At each stage and at the end, the surface of the gold electrodes was rinsed thoroughly with ultrapure water. They were dried with a gentle stream of nitrogen and then placed in an UV/ozone ProCleanerTM for 30min to eliminate any possible organic contamination.

2.3. GA-PS and GA-PS-PAMAM nanofibrous mats preparation

GA coupling agent was used to activate PAMAM dendritic polymer amine groups on the surface of NFs to allow covalent bonding with amino groups in the Fc region of anti-TNF-α. Briefly, gold electrodes containing PS and PS-PAMAM NFs were exposed to saturated GA vapors in the desiccator for 2h.

2.4. Antibodies and Antigens standard solutions preparation

The anti-TNF-α and AgTNF-α have been reconstituted in PBS buffer (10 mM, pH 7.4) and then aliquoted at 20 µL according to the protocol provided by the supplier to get a stock solution with a final concentration of 500 µg/mL and 100 µg/mL, respectively. The aliquots were stored at -20°C until use. The anti-TNF-α solution was diluted at 10 µg/mL in PBS (10 mM, pH 7.4). The standard solutions containing of AgTNF-α were prepared at five different concentrations (10, 25, 50,100, and 200 pg/mL) by dissolving the appropriate amount of the stock solution in PBS (10 mM, pH 7.4) and stored at 4°C. All the standard solutions were prepared by weighing.

2.5. immunosensor preparation

Immunosensor construction was done by pipetting 50 µl of anti-TNF-α (10 µg/mL) on the surface of NFs and then incubating for 1h at 4°C. After this step, the electrode surface was gently washed three times with PBS (10 mM, pH 7.4) to eliminate unbound antibodies from the NFs 's surface. Finally, blocking treatment for reducing non-specific binding and blocking remaining active sites was done by pipetting 100 µl of BSA 1% solution on the NFs and incubating for 1h at 4°C.

2.7 Electrochemical measurements

For the detection of AgTNF-α, the NFs modified gold electrode was subjected to successive immobilization with standard solutions (50µl) containing different concentrations of AgTNF-α prepared as described in the section 2.4 for 30min at RT (20 ± 1°C) in the electrochemical cell, followed by PBS washing to remove unbounded AgTNF-α cytokine. At each AgTNF-α concentration, an EIS response was then recorded by filling the cell with 5ml of 5mM of $K_3Fe(CN)_6/K_4Fe(CN)_6$ in PBS buffer at pH 7.4. After each EIS

measurement, the electrolyte solution in the cell was removed and the cell were washed with PBS solution to remove all adsorbed electrolyte solution from surface of NFs and prevent denaturation of anti-TNF-α.

3. Results and discussion

3.1. Characterization of nanofibrous mats

3.1.1. FTIR Spectroscopy

The ATR-FTIR spectra of PS and PS-PAMAM NFs with different concentrations are presented in Fig. 1. The bands at 3080-3024, 2920, and 2846 cm^{-1} associated with the aromatic C-H stretching vibration absorption and the existence of CH_2, respectively were found in the spectrum of pure PS NFs. Also, the peaks at 1939, 1869, 1801, and 1741 cm^{-1} were representative to overtone aromatic. The C=C stretching vibration absorption were seen at 1600 cm^{-1} and bending vibrations of CH_2 were observed at 1492, and 1451 cm^{-1}. The absorption peaks at 755 and 696 cm^{-1} associated with C-H out-of-plane bending vibration absorption were also seen. In comparison to pure PS, the amine and amide peaks of PAMAM emerged in the spectra of NFs containing dendrimer. The spectrum of PS- PAMAM NFs with different mass ratio along with characteristic PS peaks exhibited a new peak at 3268 cm^{-1} correspond to N-H stretching vibration. The C=O of amide I band, N-H bending and C-N stretch of amide II band, and C-N stretch of amide III bands appeared at peaks of 1645, 1551, and 1372 cm^{-1}, respectively. In addition, the peaks at 1155 and 1122 cm^{-1} that belong to the C-N stretch of amine were found. The peak at 2810 cm^{-1} due to the stretching bands of C-H close to NH group was observed. The intensity of the mentioned peaks increases as dendrimer concentrations increase, confirming the existence of more dendrimer on the PS-PAMAM NFs surface.

3.1.2. Morphological Studies

In order to evaluate NFs in terms of diameter, uniformity, and the effect of PAMAM dendritic polymer on PS morphology, FE-SEM micrographs were prepared. Fig. 2a and b demonstrate FE-SEM micrographs of PS NFs at two magnifications, with the average diameter of 985±303 nm. Fig. 2c and d show micrographs of PS-PAMAM NFs (65-35), which have significantly reduced fiber diameters compared to pure PS. This

decrease in diameter is due to a decrease in solution viscosity, increasing the conductivity of electrospinning solution and surface charge density of ejected jet with increasing dendrimer ratio due to low molecular weight and the cationic characteristic of PAMAM dendritic polymer, respectively, whereby the polymer jet is subjected to more elongation force in a constant electric field. This increase in elongation is also evident in the morphology of the NFs so that the porosity of the PS nanofiber surface was disappeared and the surface became smoother. Table 1 shows the results of the electrical conductivity of electrospinning solutions. According to the results, the electrical conductivity of the PS solution was 0.4 μS/cm, while it reached 24.0 μS/cm in the sample 65-35. The diameter of PS-PAMAM NFs with ratios of 85-15, 75-25, and 65-35 were 350±126 nm, 319±86 nm, and 295±94 nm, respectively. Significant results can be summarized based on the morphology of the resulting NFs. (1) Modification with PAMAM has substantially decreased the diameter and increased the accessible surface area of the resultant NFs compared to pure PS, allowing more anti-TNF-α to be immobilized on the surface and increasing the immunosensor's sensitivity. (2) The uniformity of the diameter, whether in a single fiber or in the average diameter of the fibers, as well as the bead-less morphology, contribute to immunosensor reproducibility. (3) The porous structure of the NFs mats allows the desired analyte to access even the immobilized bioreceptor in the lower layers of the fibers, and provides no penetration resistance. (4) The morphology of PS NFs has not changed after doping with PAMAM dendritic polymer, which is a benefit for the creation of reproducible immunosensors.

3.1.3. Water contact angle

The images of the water droplets on the pure PS and PS-PAMAM NFs (65-35) on the surface of the gold electrode are inserted in Fig. 2. Pure PS NFs showed a contact angle of 147.2±1.1°, which is due to the lack of functional groups in their structure and their hydrophobic nature. The contact angles of samples 85-15, 75-25, and 65-35, have been greatly reduced to 48.2±1.2°, 31.8±1.3°, and 15.4±1.2°, respectively. According to the results, the presence of PAMAM in the structure of NFs on the one hand reduces the diameter of fibers and increases their surface area and, on the other hand, increases more hydrophilic amine

groups on the surface of PS NFs, both of which play an effective role in NFs surface properties. As a result of the high hydrophobicity of PS and absence of functional groups on its surface, there is a lack of homogeneous distribution of anti-TNF-α on the fiber surface, as well as covalent bonding with the NFs' surface. In PS-PAMAM samples, increasing the concentration of the PAMAM provides increased hydrophilicity and higher functional groups to the anti-TNF-α on a more uniform immobilization at the fiber surface. Regardless of the chemical structure and morphology of NFs and only based on the shape of the water droplet on the NFs surface in Fig. 2, unlike the PS sample, the droplet in the PS-PAMAM (65-35) spread well on the surface. While the procedures of immobilizing anti-TNF-α on the surface of the fibers were accomplished by pipetting a specific quantity of antibody onto the fibers' surface, the hydrophilic properties of PS-PAMAM fibers allow for more uniform antibody immobilization. However, immobilization of anti-TNF-α on the surface of PS NFs confined to the droplet's position. To examine the surface properties of NFs following treatment with GA and anti-TNF-α immobilization, the contact angle of the NFs was measured (Table 1). The contact angle increased after applying PS-PAMAM NFs with GA owing to the interaction of dendrimers amine groups on the surface of NFs with GA and the formation of Schiff bases. The contact angle of sample 65-35 rose from 15.4±1.2° to 35.9±4.7°after treatment with GA, indicating that GA forms covalent bonds with amine groups. However, the contact angle of PS NFs did not change after GA treatment due to the lack of amine groups at their surface. The contact angle fell to 16.4±2.5° after immobilization of anti-TNF-α on sample 65-35, indicating that antibodies were immobilized at the fiber surface. This trend has been true for samples 85-15 and 75-25. The slight decrease in the contact angle observed in the PS sample is related to the grafting of the anti-TNF-α on the surface of the NFs.

3.2. Immunodetection and Interference of TNF-α cytokines

The Cyclic voltammograms (CVs) were performed in 10 mM PBS (pH 7.4) with 5.0 mM $[Fe(CN)_6]^{3-/4-}$ as the redox probe from −0.2 to +0.6 V and the scan rate of 60 mV/s to provide more specific information about electrodes containing NFs and to analyze electrode behavior changes throughout stepwise

immunosensor fabrication. As shown in Fig. 3a, the PS-PAMAM NFs with different concentrations exhibit a couple of reversible redox peaks. As the concentration of PAMAM increases, the peak current increases, which is related to the increase in effective surface area with decreasing fiber diameter as well as the effect of dendrimer on electron transfer. The disappearance of the oxidation and reduction peaks of the redox couple in the pure PS NFs is related to their non-conducting properties, large diameter, and high hydrophobicity. How PAMAM improves electron transfer in NFs is better understood by imagining a network of it within a 3D nanofiber and on its surface that some of them face the working electrode and the others facing the solution. This indicates that from a certain concentration onwards the amount of PAMAM reaches a critical level to form a network within the NFs and on their surface, which increases the electron transfer. This network is well-formed in sample 75-25, and with increased dendrimer concentration and decreasing fiber diameter (sample 65-35), more PAMAM will be present on the surface of the fibers, resulting in enhanced electron transport. Surface modification of the glassy carbon electrode with PAMAM produced similar outcomes in terms of increased electric flux, improved conductive capacity, noise reduction, and faster electron transfer processes on the electrode's surface [19].

The redox current of $[Fe(CN)_6]^{3-/4-}$ after electrospinning of NFs (65-35) on the electrode surface (129.3 μA) has increased compared to the bare gold electrode (116.7 μA) due to the increase in high specific surface area and improved charge-transport by the PAMAM (Fig. 3b). After the immobilization of the anti-TNF-α and blocking with BSA, the redox current (111.2 μA) has decreased due to the formation of a layer of protein molecules on the surface of the fibers that insulate the electrode and prevent electron transmission between electrode and electrolyte. This confirms the ability of the substrate to immobilize anti-TNF-α. Antibody activity on the surface of NFs was assessed by incubating 50 μl AgTNF-α (10 pg/mL) on the electrode surface for 30 min. The decrease in redox current (102.7 μA) and increase in peak-to-peak separation in voltammogram confirm the immunosensor is highly sensitive to TNF-α cytokine through the formation of immune complexes that could hinder electron transfer between the electrode and the electrolyte as insulating biomolecules.

Electrodes containing sample 65-35 NFs with 4 different deposition durations of 1, 2, 3, and 5 min were studied using SEM and CV to discover the ideal electrospinning time and to evaluate the influence of deposit time on the redox current of $[Fe(CN)_6]^{3-/4-}$. Increasing the electrospinning duration induces more NFs to deposit, resulting in a thicker layer mat, as seen in Fig. S 1 (SI). The remarkable point in the images is the uniform diameter and the beaded-free structure of the NFs mats in different samples. This reaffirms the developed immunosensor is reproducible. The CV results show a decreasing trend in redox current with increasing electrospinning time (Fig. S 2). It is related to increasing the thickness of the NFs mats and decreasing the porosity between the NFs, which prevents penetration of $[Fe(CN)_6]^{3-/4-}$ to the electrode surface. The 1 min electrospinning was selected as the ideal time due to the following reasons. (1) having the highest current intensity in comparison to others, (2) supplying the appropriate and adequate quantity of NFs on the electrode surface, and (3) having the best adherence to the electrode surface and suitable stability throughout immobilization, blocking, and washing processes. Despite the role of the PAMAM in the good adhesion of NFs to the electrode surface, increasing the electrospinning duration leads the NFs to be attached only with their bottom layer and not in touch with the electrode surface. As a result, 1 min of electrospinning was chosen as the optimal time, and all immunosensors were made using this time.

The EIS was utilized to quantitatively analyze the performance and sensitivity of the developed immunosensor in detecting TNF-α cytokine and confirming the formation of immune complexes between anti-TNF-α and AgTNF-α on the NFs surface. The acquired Nyquist impedance plots for developed immunosensors are shown in Fig.4, where the charge transfer resistance at the electrode surface (Rct) is proportional to the semi-circle diameter. The first semi-circle relates to anti-TNF-α immobilization on the surface of NFs at 4 °C for 1h. After this step, the immunosensors were evaluated to detect AgTNF-α in the concentration range of 10-200 pg/ml. The Nyquist plot of an immunosensor based on pure PS NFs is shown in Fig. 4a. Because of the lack of functional groups on the surface of pure PS NFs, it is not feasible to immobilize antibodies uniformly and covalently on these NFs. Only the anti-TNF-α was physically attached to the NFs' surface, leading to antibody accumulation, denaturation, and desorption at different sensing

stages. The immunosensor did not work and the semi-circles did not increase due to a low amount of immobilized anti-TNF-α and saturation of them on the surface of PS NFs. The Nyquist plots of PS-PAMAM NFs with different mass ratios 85-15, 75-25, and 65-35 are shown in Figures 4b-d. The semi-circles gradually increased with increasing the AgTNF-α content in all PS-PAMAM NFs samples, indicating AgTNF-α biorecognition with anti-TNF-α on the surface of NFs. By comparing the semi-circle and linear part of the impedance spectra of the immunosensors, a smaller semi-circle with better diffusion of $[Fe(CN)_6]^{3-/4-}$ toward the surface of the electrode is observed with increasing PAMAM dendritic polymer concentration. This is due to decreased diameter and increased hydrophilicity, and the presence of PAMAM on the NFs surface, which enhances charge transfer for $[Fe(CN)_6]^{3-/4-}$. This is in line with the findings of the CV of NFs with different PAMAM concentrations. After each step, the electrochemical parameters were calculated by fitting the Nyquist plot with Randles equivalent circuit, which provided the best fit for the impedance parameters (Fig.4 inset). It consists of electrolyte resistance (R_s) in series with a parallel combination of constant phase element Q_{CPE} and charge transfer resistance (R_{ct}). The calibration curve of developed immunosensors was drawn based on $(R_{(antibodies)}–R_{(antigens)})/R_{(antibodies)}$ obtained from the equivalent circuit against the logarithmic value of the AgTNF-α concentration (Fig. 4e). The calibration graph of PS-PAMAM NFs-based immunosensors showed a linear correlation in ranges between 10 - 200 pg/mL. Increasing the concentration of PAMAM has increased the slope of the graph and the higher detection sensitivity of the immunosensor due to the higher loading of antibodies on the surface of NFs. In comparison to the other samples, PS-PAMAM with the concentration of 65-35 has the highest slope, with a linear regression equation of $\Delta R/R = 0.379 \ln [AgTNF-\alpha]-0.461$ and a correlation coefficient of $R^2 = 0.987$, indicating that this immunosensor has a higher sensitivity to antigen changes due to the higher presence of PAMAM and immobilization of antibodies on the surface of NFs.

The LOD of immunosensor was 669 fg/mL based on 3.S/m, where S is the residual standard deviation and m is the slope of the regression line. The trend is similar in samples 85-15 and 75-25, but they have a lower slope than samples 65-35: $\Delta R/R = 0.210 \ln [AgTNF-\alpha]-0.132$ for sample 85-15 and $\Delta R/R = 0.2680 \ln$

[AgTNF-α]-0.235 for sample 75-25. Table S1 compares the detection range and LOD of the developed immunosensor to those of previous electrochemical TNF-α immunosensors.

Table S1 compares the prepared immunosensor to previously reported literature in detail. The immunosensor has a wide linear detection range with the lowest LOD than previous electrochemical TNF-α cytokine immunosensors. This is rooted in the high surface-to-volume ratio of NFs and allows antibodies to be covalently immobilized with a significantly higher density on the fiber surface, a high accessibility due to the porous structure. The electrospun NFs-based immunosensor produced in this study provided a flexible interface with a low-cost and simple production method, allowing the development of a new generation of immunosensors for insertion in a point of care testing.

The selectivity of the PS-PAMAM NFs-based immunosensor was also considered as a significant property of immunosensors. For this, all of the procedures used for AgTNF-α were repeated for cytokines IL-10 (Fig. 4f). According to the results, the developed immunosensor had higher selectivity and sensitivity to AgTNF-α compared to IL-10.

4. Conclusion

Nanostructured transducers along with the ideal surface chemistry design can lead to the development of highly sensitive immunosensors. In this work, a PS-PAMAM NFs-based immunosensor was developed that provided the ideal protein-friendly platform with a high surface area and a well-designed receptor surface for the immobilization of anti-TNF-α. The role of PAMAM dendritic polymer and its presence on the fiber surface at three different concentrations were investigated and sample 65-35 had the highest sensitivity and linear response for AgTNF-α due to the higher presence of dendrimer on the surface. This highly sensitive immunosensor, along with the easy and fast preparation method, provided conditions for the anti-TNF-α to be covalently immobilized on the fiber surface without losing their activity to detect the AgTNF-α with high sensitivity. This could be promising for the development of a point of care and flexible immunosensor with maximum analyte detection ability.

Acknowledgements

P.R. thanks the Ministry of Science, Research and Technology of the Islamic Republic of Iran for providing the scholarship. The authors acknowledge the financial support of the European Union's Horizon 2020 research and innovation programme, Project NMBP-13-2017 KardiaTool (Grant agreement No.768686) and POC4Allergies (Ref.ERAPERMED2019-127).

References

[1] E.B. Aydın, M. Aydın, M.K. Sezgintürk, A highly sensitive immunosensor based on ITO thin films covered by a new semi-conductive conjugated polymer for the determination of TNFα in human saliva and serum samples, Biosens. Bioelectron. 97 (2017) 169–176. https://doi.org/10.1016/j.bios.2017.05.056.

[2] Y.K. Bahk, H.H. Kim, D.S. Park, S.C. Chang, J.S. Go, A new concept for efficient sensitivity amplification of a QCM based immunosensor for TNF-α by using modified magnetic particles under applied magnetic field, Bull. Korean Chem. Soc. 32 (2011) 4215–4220. https://doi.org/10.5012/bkcs.2011.32.12.4215.

[3] D. Vozgirdaite, H. Ben Halima, F.G. Bellagambi, A. Alcacer, F. Palacio, N. Jaffrezic-Renault, N. Zine, J. Bausells, A. Elaissari, A. Errachid, Development of an immunoFET for analysis of tumour necrosis factor-α in artificial saliva: Application for heart failure monitoring, Chemosensors. 9 (2021) 1–12. https://doi.org/10.3390/chemosensors9020026.

[4] M. Bahri, A. Baraket, N. Zine, M. Ben Ali, J. Bausells, A. Errachid, Capacitance electrochemical biosensor based on silicon nitride transducer for TNF-α cytokine detection in artificial human saliva: Heart failure (HF), Talanta. 209 (2020) 120501. https://doi.org/10.1016/j.talanta.2019.120501.

[5] A.K. Yagati, M. Lee, J. Min, Bioelectrochemistry Electrochemical immunosensor for highly sensitive and quantitative detection of tumor necrosis factor- α in human serum, Bioelectrochemistry. 122 (2018) 93–102. https://doi.org/10.1016/j.bioelechem.2018.03.007.

[6] Z. Sun, L. Deng, H. Gan, R. Shen, M. Yang, Y. Zhang, Biosensors and Bioelectronics Sensitive immunosensor for tumor necrosis factor a based on dual signal amplification of ferrocene modified self-assembled peptide nanowire and glucose oxidase functionalized gold nanorod, Biosens. Bioelectron. 39 (2013) 215–219. https://doi.org/10.1016/j.bios.2012.07.050.

[7] E. Sánchez-Tirado, C. Salvo, A. González-Cortés, P. Yáñez-Sedeño, F. Langa, J.M. Pingarrón, Electrochemical immunosensor for simultaneous determination of interleukin-1 beta and tumor necrosis factor alpha in serum and saliva using dual screen printed electrodes modified with functionalized double–walled carbon nanotubes, Anal. Chim. Acta. 959 (2017) 66–73. https://doi.org/10.1016/j.aca.2016.12.034.

[8] M. Qi, Y. Zhang, C. Cao, M. Zhang, S. Liu, G. Liu, Decoration of Reduced Graphene Oxide Nanosheets with Aryldiazonium Salts and Gold Nanoparticles toward a Label-Free Amperometric Immunosensor for Detecting Cytokine Tumor Necrosis Factor-α in Live Cells, Anal. Chem. 88 (2016) 9614–9621. https://doi.org/10.1021/acs.analchem.6b02353.

[9] L. Barhoumi, A. Baraket, F.G. Bellagambi, G.S. Karanasiou, M. Ben Ali, D.I. Fotiadis, J. Bausells, N. Zine, M. Sigaud, A. Errachid, A novel chronoamperometric immunosensor for rapid detection of TNF-A in human saliva, Sensors Actuators, B Chem. 266 (2018) 477–484. https://doi.org/10.1016/j.snb.2018.03.135.

[10] Z. Yin, Y. Liu, L. Jiang, J. Zhu, Biosensors and Bioelectronics Electrochemical immunosensor of tumor necrosis factor ⌴ based on alkaline phosphatase functionalized nanospheres, Biosens. Bioelectron. 26 (2011) 1890–1894. https://doi.org/10.1016/j.bios.2010.03.025.

[11] E.B. Bahadir, M.K. Sezgintürk, Poly(amidoamine) (PAMAM): An emerging material for electrochemical bio(sensing) applications, Talanta. 148 (2016) 427–438. https://doi.org/10.1016/j.talanta.2015.11.022.

[12] M. Hasanzadeh, N. Shadjou, M. Eskandani, J. Soleymani, F. Jafari, M. de la Guardia, Dendrimer-encapsulated and cored metal nanoparticles for electrochemical nanobiosensing, TrAC - Trends Anal. Chem. 53 (2014) 137–149. https://doi.org/10.1016/j.trac.2013.09.015.

[13] M. Elancheziyan, K. Theyagarajan, D. Saravanakumar, K. Thenmozhi, S. Senthilkumar, Viologen-terminated polyamidoamine (PAMAM) dendrimer encapsulated with gold nanoparticles for nonenzymatic determination of hydrogen peroxide, Mater. Today Chem. 16 (2020) 100274. https://doi.org/10.1016/j.mtchem.2020.100274.

[14] S. Chandra, C. Gäbler, C. Schliebe, H. Lang, D. Bahadur, Fabrication of a label-free electrochemical immunosensor using a redox active ferrocenyl dendrimer, New J. Chem. 40 (2016) 9046–9053. https://doi.org/10.1039/c6nj00830e.

[15] B. Liu, M. Li, Y. Zhao, M. Pan, Y. Gu, W. Sheng, G. Fang, S. Wang, A sensitive electrochemical immunosensor based on PAMAM dendrimer-encapsulated Au for detection of norfloxacin in animal-derived foods, Sensors (Switzerland). 18 (2018). https://doi.org/10.3390/s18061946.

[16] Y. Liu, Q. Zhang, H. Wang, Y. Yuan, Y. Chai, R. Yuan, An electrochemiluminescence immunosensor for thyroid stimulating hormone based on polyamidoamine-norfloxacin functionalized Pd-Au core-shell hexoctahedrons as signal enhancers, Biosens. Bioelectron. 71 (2015) 164–170. https://doi.org/10.1016/j.bios.2015.04.022.

[17] C.A. Razzino, V. Serafín, M. Gamella, M. Pedrero, A. Montero-Calle, R. Barderas, M. Calero, A.O. Lobo, P. Yáñez-Sedeño, S. Campuzano, J.M. Pingarrón, An electrochemical immunosensor using gold nanoparticles-PAMAM-nanostructured screen-printed carbon electrodes for tau protein determination in plasma and brain tissues from Alzheimer patients, Biosens. Bioelectron. 163 (2020) 1–8. https://doi.org/10.1016/j.bios.2020.112238.

[18] A. Bosnjakovic, M.K. Mishra, H.J. Han, R. Romero, R.M. Kannan, A dendrimer-based immunosensor for improved capture and detection of tumor necrosis factor-α cytokine, Anal. Chim. Acta. 720 (2012) 118–125. https://doi.org/10.1016/j.aca.2012.01.017.

[19] B. Zhang, B. Liu, G. Chen, D. Tang, Redox and catalysis “all-in-one” infinite coordination polymer for electrochemical immunosensor of tumor markers, Biosens. Bioelectron. 64 (2015) 6–12. https://doi.org/10.1016/j.bios.2014.08.024.

Figure Captions

Schematic.1. The schematic of the stepwise preparation process of NFs based EIS immunosensor.

Fig. 1. ATR-FTIR spectra of (a) pure PS, (b) PS-PAMAM-(85-15), (c) PS-PAMAM-(75-25), and (d) PS-PAMAM-(65-35) NFs.

Fig. 2. FE-SEM images of (a) and (b) pure PS, (c) and (d) PS-PAMAM-(65-35) NFs, and (e) diameter distribution histograms of NFs. Insets in Fig.2 are the images of water droplets on the surface of electrospun NFs on a gold electrode.

Fig. 3. CVs of (a) pure PS and PS-PAMAM NFs with different concentrations, (b) bare gold, gold electrode containing PS-PAMAM-(65-35) NFs, anti-TNF-α -GA-PS-PAMAM-(65-35) NFs, and AgTNF-α -anti-TNF-α- GA-PS-PAMAM-(65-35) in a 10 mM PBS (pH 7.2) containing 5.0 mM $[Fe(CN)_6]^{3-/4-}$ (scan rate = 60 mV/s).

Fig. 4. Nyquist plots of impedance spectra obtained in 10 mM PBS (pH 7.4) solution containing 5mM $[Fe(CN)_6]^{3-/4-}$ for gold electrodes containing (a) pure PS, (b) PS-PAMAM-(85-15), (c) PS-PAMAM-(75-25), and (d) PS-PAMAM-(65-35) NFs for AgTNF-α detection ranging from 10-200 pg/mL. EIS: polarization potential of 0.2 V vs Ref, 1 Hz–100 kHz frequency range, and a sinus amplitude of 10 mV. Inset was the equivalent circuit model used to fit the impedance data. (e) calibration curves of the developed immunosensors for the detection of AgTNF-α cytokine. (f) Selectivity histograms of the developed immunosensors for the detection of Ag-TNF-α and IL-10 cytokine.

Table. 1. The characteristics of electrospinning solutions conductivity, diameter of NFs, and water contact angle of NFs on the surface of the gold electrode (a) before GA treatments, (b) after GA treatments, and (c) after anti-TNF-α immobilization.

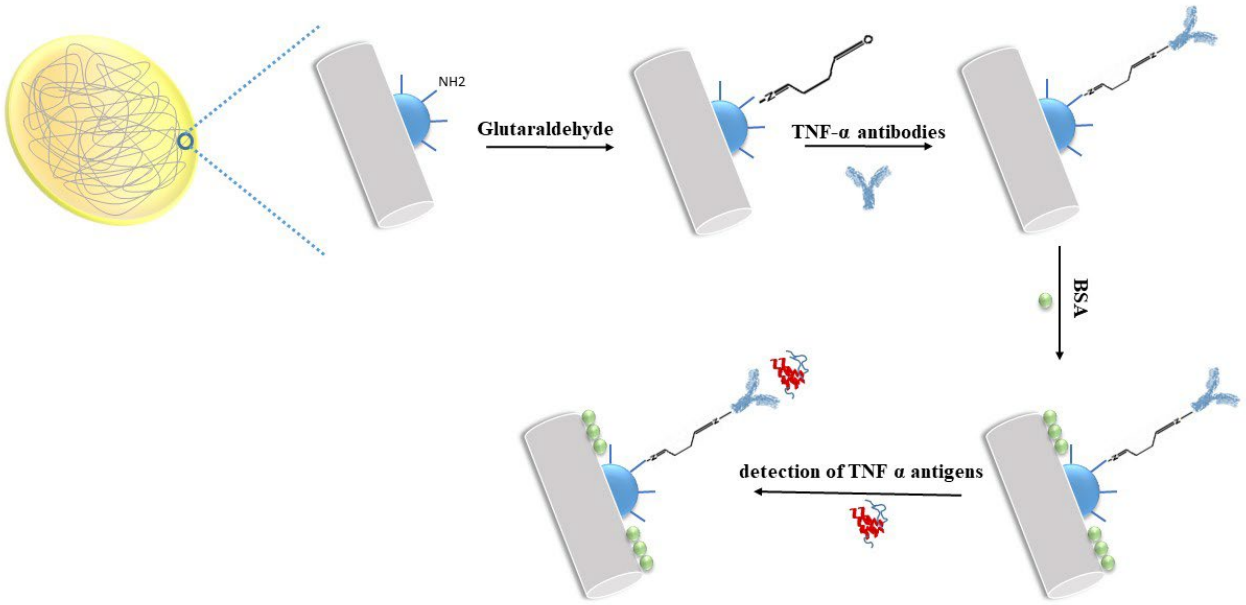

400

401

402 **Schematic.1.**

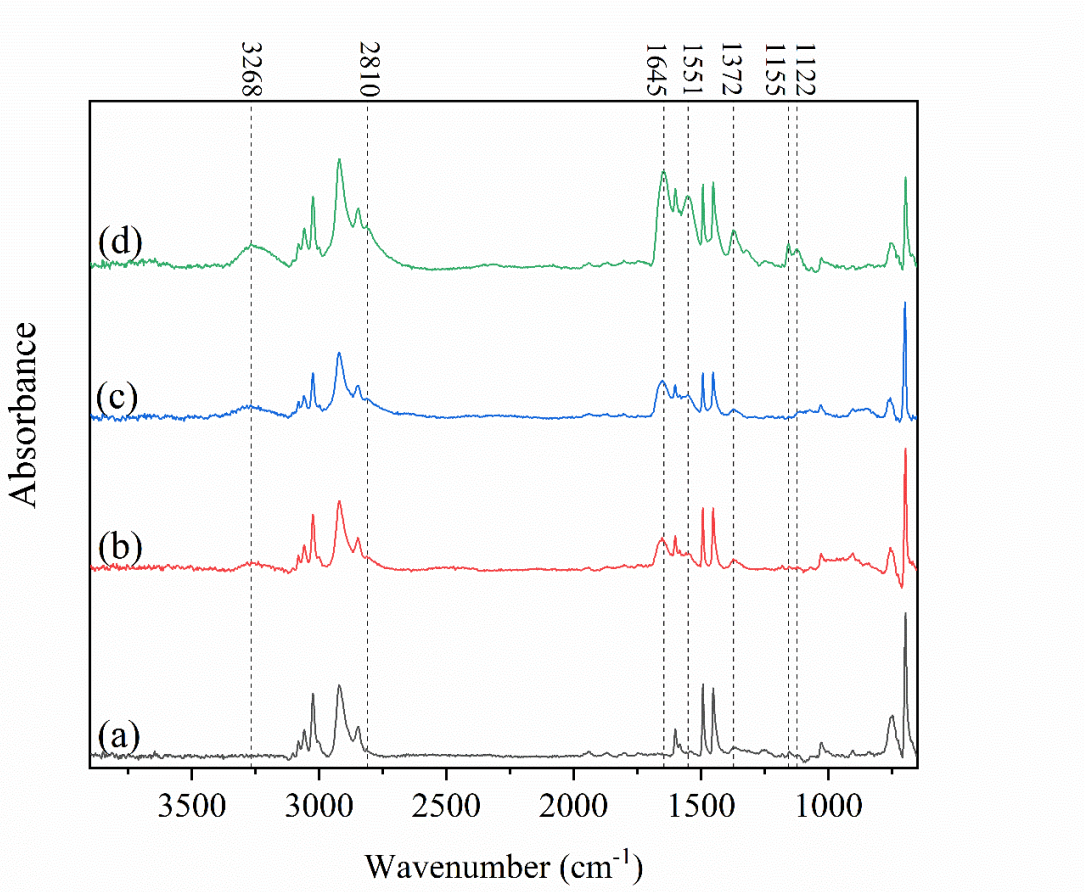

403

404 **Fig. 1.**

405

406

407

408

409

410

411

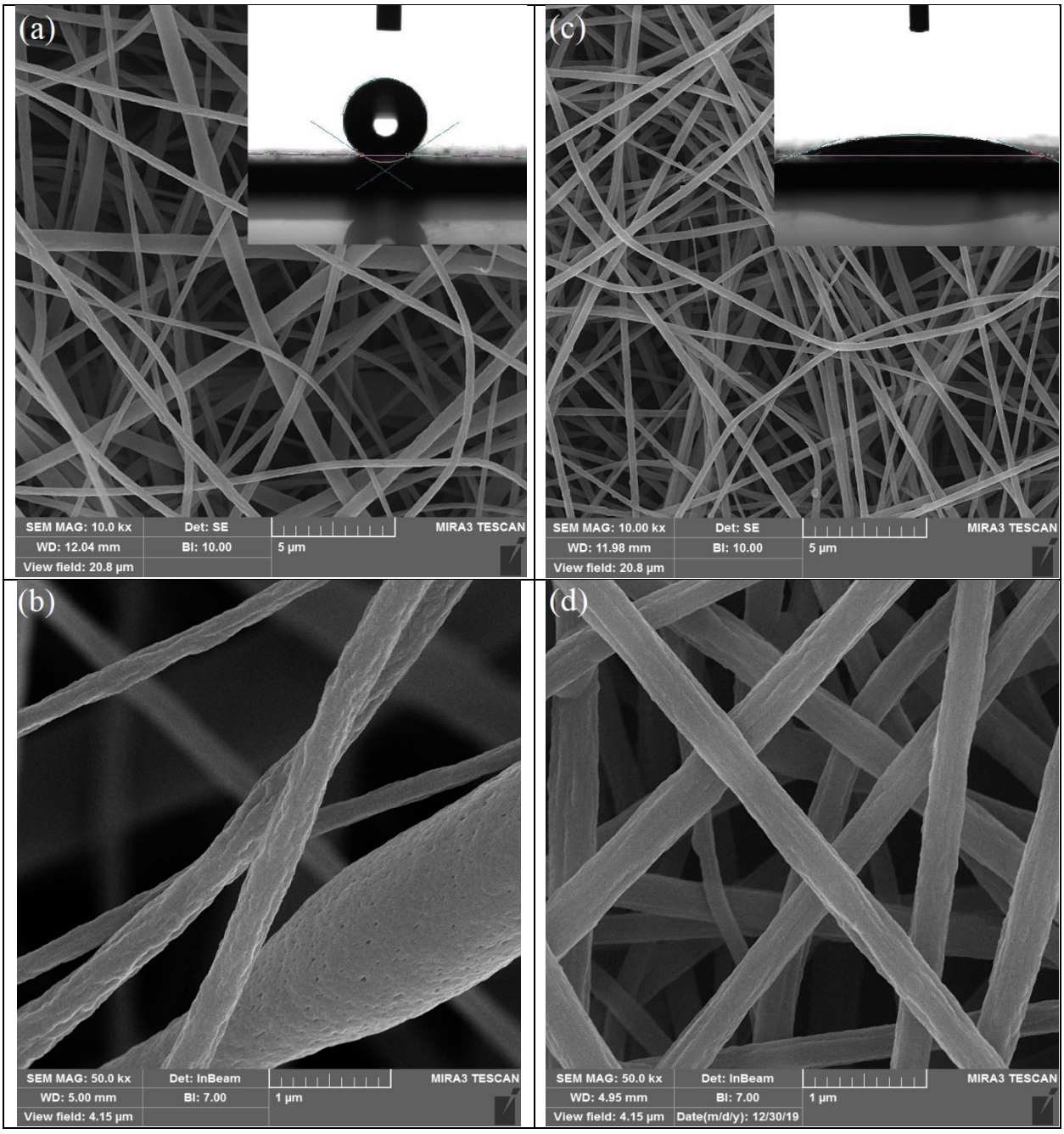
(a)
SEM MAG: 10.0 kx
Det: SE
MIRA3 TESCAN
WD: 12.04 mm
BI: 10.00
5 µm
View field: 20.8 µm
(c)
SEM MAG: 10.00 kx
Det: SE
MIRA3 TESCAN
WD: 11.98 mm
BI: 10.00
5 µm
View field: 20.8 µm
(b)
SEM MAG: 50.0 kx
Det: InBeam
MIRA3 TESCAN
WD: 5.00 mm
BI: 7.00
1 µm
View field: 4.15 µm
(d)
SEM MAG: 50.0 kx
Det: InBeam
MIRA3 TESCAN
WD: 4.95 mm
BI: 7.00
1 µm
View field: 4.15 µm
Date(m/d/y): 12/30/19

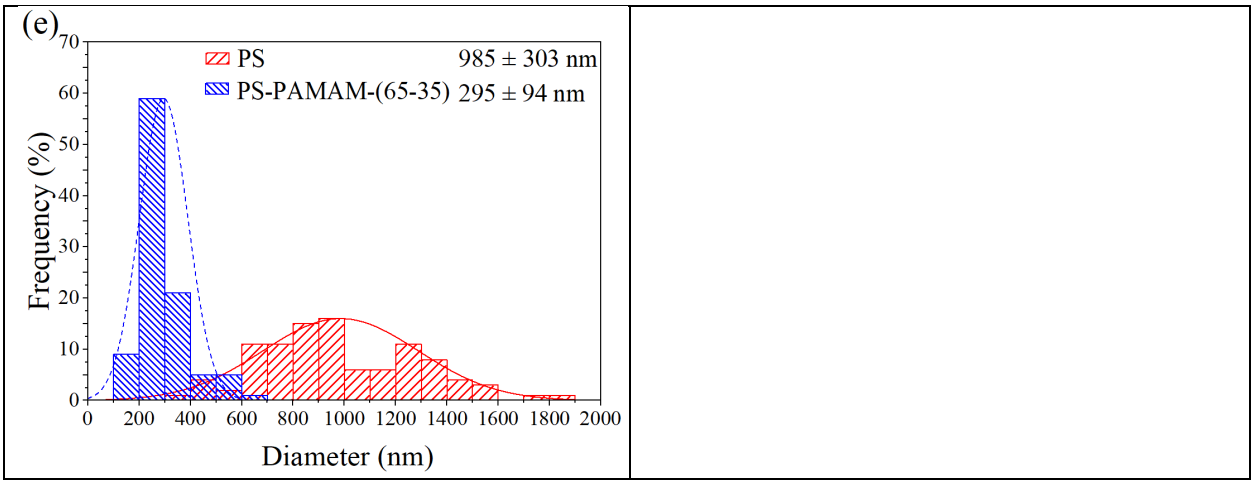
(e)
PS
985 ± 303 nm
PS-PAMAM-(65-35)
295 ± 94 nm
Frequency (%)
Diameter (nm)
0
10
20
30
40
50
60
70
0
200
400
600
800
1000
1200
1400
1600
1800
2000

Fig. 2.

Table 1.

Samples	Diameter (nm)	Conductivity (μS/cm)	Water contact angle		
			before GA	after GA	after TNF-α Ab
PS	985±303	0.4	147.2±1.1°	146.9±1.8°	132.4±2.5°
PS-PAMAM-(85-15)	350±126	11.5	48.2±1.2°	55.9±5.0°	31.4±2.3°
PS-PAMAM-(75-25)	319±86	18.2	31.8±1.3°	42.8±4.8°	28.9±3.3°
PS-PAMAM-(65-35)	295±94	24.0	15.4±1.2°	35.9±4.7°	16.4±2.5°

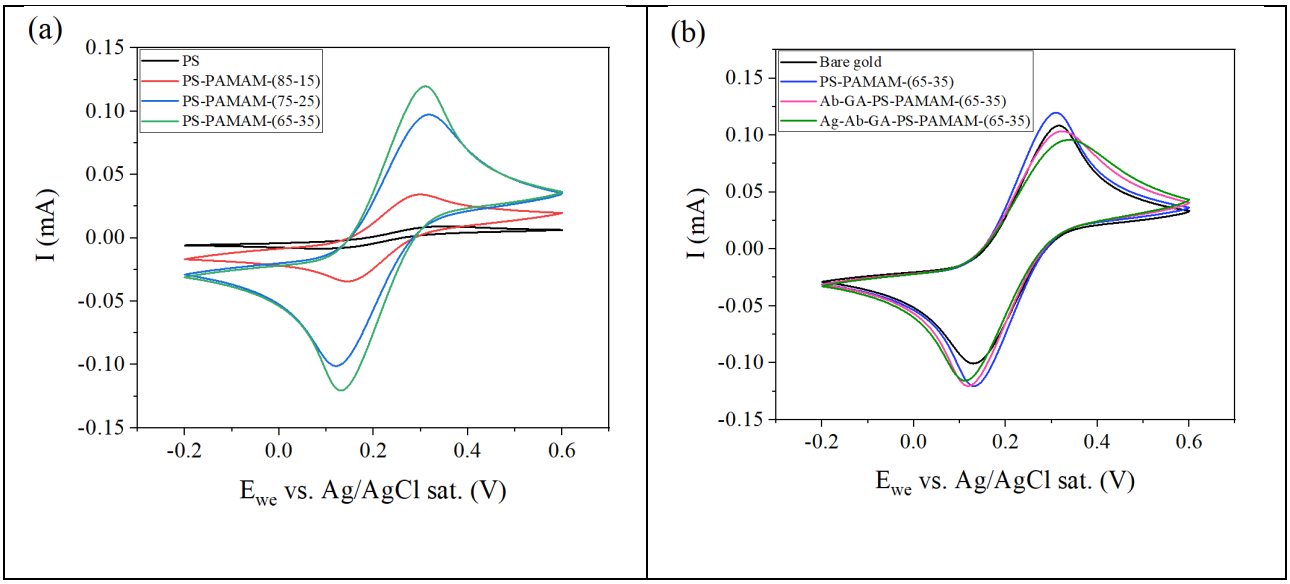
(a)
PS
PS-PAMAM-(85-15)
PS-PAMAM-(75-25)
PS-PAMAM-(65-35)
I (mA)
E$_{we}$ vs. Ag/AgCl sat. (V)
(b)
Bare gold
PS-PAMAM-(65-35)
Ab-GA-PS-PAMAM-(65-35)
Ag-Ab-GA-PS-PAMAM-(65-35)
I (mA)
E$_{we}$ vs. Ag/AgCl sat. (V)

Fig. 3.

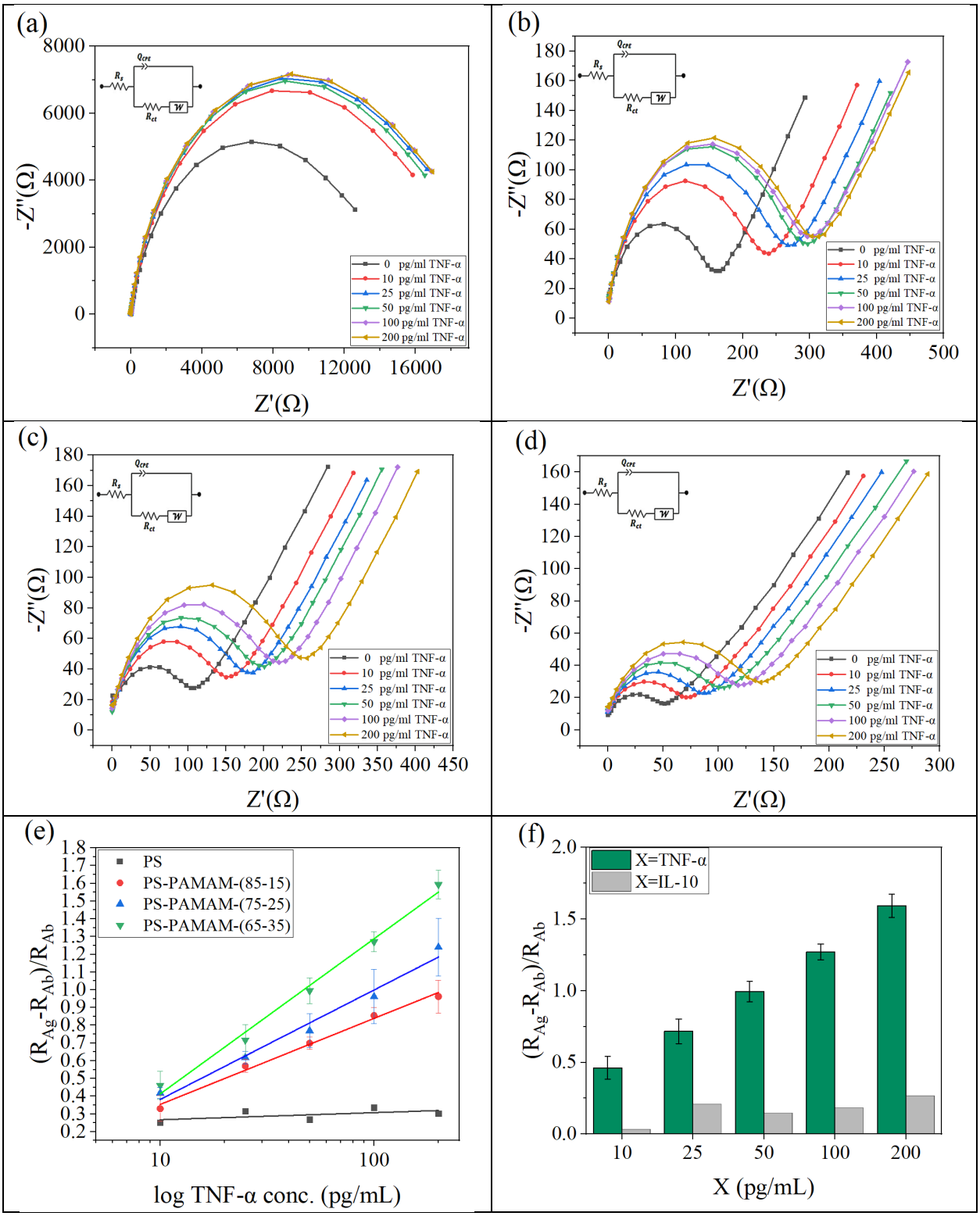
(a)
-Z''(Ω)
Z'(Ω)
0 pg/ml TNF-α
10 pg/ml TNF-α
25 pg/ml TNF-α
50 pg/ml TNF-α
100 pg/ml TNF-α
200 pg/ml TNF-α
(b)
-Z''(Ω)
Z'(Ω)
(c)
-Z''(Ω)
Z'(Ω)
(d)
-Z''(Ω)
Z'(Ω)
(e)
PS
PS-PAMAM-(85-15)
PS-PAMAM-(75-25)
PS-PAMAM-(65-35)
(R_Ag-R_Ab)/R_Ab
log TNF-α conc. (pg/mL)
(f)
X=TNF-α
X=IL-10
(R_Ag-R_Ab)/R_Ab
X (pg/mL)

Fig. 4.

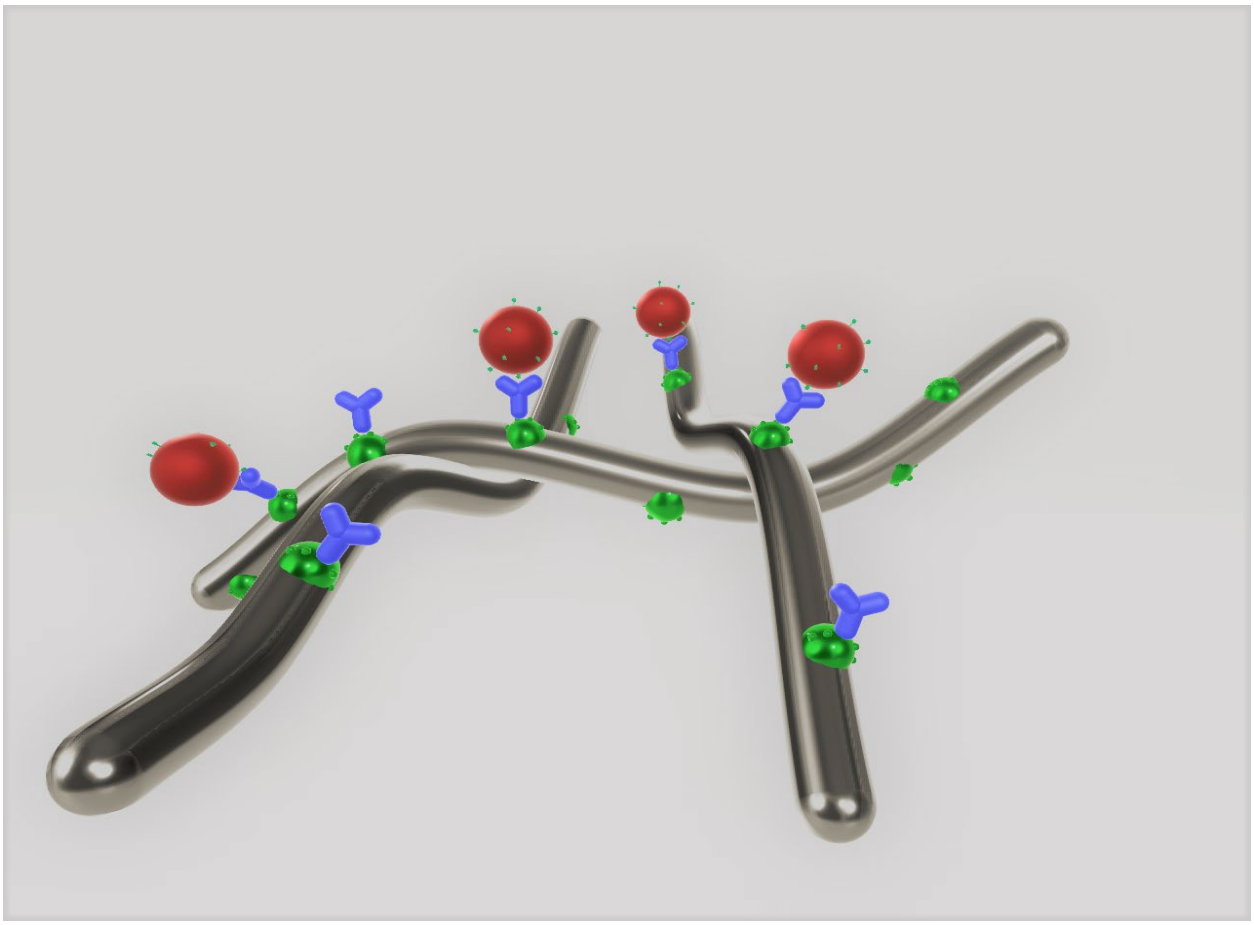

Graphical abstract